

# A three-dimensional enriched finite element method for nonlinear transient heat transfer in functionally graded materials

Mustapha Malek<sup>1</sup>, Nouh Izem<sup>1</sup>, M Shadi Mohamed<sup>2</sup>, Mohammed Seaid<sup>3,\*</sup>

<sup>1</sup> *Laboratory of Engineering Sciences, Faculty of Science, Ibn Zohr University Agadir, Morocco*

<sup>2</sup> *School of Energy, Geoscience, Infrastructure and Society, Heriot-Watt University, Edinburgh EH14 4AS, UK*

<sup>3</sup> *Department of Engineering, Durham University, Durham DH1 3LE, UK*

## Abstract

Nonlinear transient heat transfer in functionally graded materials is being studied more popular in present. In preliminary design, this problem can be simplified as a composite, and a three-dimensional transient heat transfer analysis is used to adjust dimensions of the considered materials. This paper is concerned with the numerical modeling of transient heat transfer in composite materials where the thermal conductivity is also dependent on the temperature; hence the problem is nonlinear. We are interested in solutions with steep boundary layers where highly refined meshes are commonly needed. Such problems can be challenging to solve with the conventional finite element method. To deal with this challenge we propose an enriched finite element formulation where the basis functions are augmented with a summation of exponential functions. First, the initial-value problem is integrated in time using a semi-implicit scheme and the semi-discrete problem is then integrated in space using the enriched finite elements. We demonstrate through several numerical examples that the proposed approach can recover the heat transfer on coarse meshes and with much fewer degrees of freedom compared to the standard finite element method. Thus, a significant reduction in the computational requirements is achieved without compromising on the solution accuracy. The results also show the stability of the scheme when using tetrahedral unstructured grids.

**Keywords.** Nonlinear heat transfer; Functionally graded material; Heterogeneous problems; Partition of unity method; Finite element discretization; Enrichment procedures

## 1 Introduction

Numerical modeling of nonlinear heat transfer in composite materials becomes very demanding if dealing with strong discontinuity in the material properties. This can be the case when considering functionally graded materials where often a highly conductive alloy is integrated with a low conductive ceramic. Thus, the numerical modeling is a serious challenge not only because of the problem nonlinearity but also due to the formation of steep boundary layers on the ceramic surface in the composites. To computationally deal with this class of problems, several finite element methods are developed where often high order basis functions are used for approximating the solution, see for example [27, 30]. In this regards, designing problem-specific basis functions have several advantages over the generic finite element basis. For instance, Trefftz-type finite elements have shown significant improvement over the standard finite elements in terms of the required number of degrees of freedom [25]. Hybrid Trefftz finite elements have also been created to

---

\*Corresponding author: m.seaid@durham.ac.uk

recover the solution in composite materials [7]. In this case, the numerical solution is approximated on two different levels such that high-order basis functions are used inside an element while standard polynomial functions are used on its boundary [4]. Note that these two independent approximation fields help to capture local effects such as discontinuities, singularities and inclusions [25].

Another closely related approach to the Trefftz finite elements is the well-known Partition of Unity Method (PUM) [16]. This method has been widely used in the literature and has found many applications in recent years. For example, a summation of exponential functions was used in the PUM to capture steep boundary layers inherited from heat transfer in homogeneous media [19, 15] and later in heterogeneous materials [2, 14] for two-dimensional applications. The presented numerical experiments in these references show clear advantages of enriching the approximation space when dealing with multiscale heat transfer problems involving local irregularities as well as steep boundary layers [19, 3, 29]. To analyze geothermal applications in large computational domains, the finite element method was also enriched with time-dependent functions that is designed to replicate the analytical solutions [29]. Thus, coarse meshes can be utilized to recover the solution with good accuracy without relying on simulations on very fine meshes. In addition, a global-local approach was developed to deal with problems involving heat transfer with a heat source localized in an area much smaller than the considered domain [22, 10]. In this case, the problem is first solved over local domains only in the vicinity of the heat source then, the numerical solution is used as a discrete function to enrich the global domain. The approach enables much coarser meshes compared to otherwise the highly refined meshes necessary to consider the localized heat sources [23, 11]. A partition of unity approach was also developed for conduction-radiation heat transfer in grey media [20] as well as in glass [21]. This approach employed a combination of time-independent hyperbolic and Gaussian functions for the enrichment to resolve the steep gradients in the numerical solution as it evolves in time. It should be stressed that for linear problems, the same matrix is retained for all time steps in the linear system inherited by PUM whereas only the right hand side of the resulting system is updated. Hence, the reduction in the computational requirements is achieved not only by using coarse elements but also by building and decomposing small size matrices which can be solved using direct solvers [19, 14, 6]. The solution of the linear system using iterative solvers was also investigated in the literature, see for instance [9, 18].

In the present study, a three-dimensional enriched finite element method is developed for solving nonlinear transient heat transfer in composites with steep boundary layers. The proposed method considers a class of exponential enrichment functions to solve the problem on coarse meshes. A semi-implicit time stepping scheme of Gear-type is used for the time integration for which only linear systems of algebraic equations are solved to update the numerical solution. Here, the enrichment functions are chosen to be time-independent so that the global matrix in the linear systems does not depend on time. To assess the numerical performance of the proposed approach, we solve a problem with known analytical solution so that the results obtained using the PUM are compared to those obtained using the standard FEM. This quantitative comparison is carried out in terms of errors and total numbers of degrees of freedom in each approach. The method is also used to recover the heat transfer in a functionally graded materials relevant to two industrial applications. Results presented in this paper show high resolution of the proposed enriched finite element method and permit the straightforward application of the method to more complex, physically based nonlinear transient heat transfer problems. The current work represents a step towards the implementation of three-dimensional enriched finite element method for the numerical solution of heat and mass transfer.

This paper is organized as follows. In section 2 the nonlinear initial value problem in composite materials is presented and the finite element weak formulation is derived. The partition of unity approximation of the solution along with the considered enrichment functions are discussed in section 3. In section 4, we examine the numerical performance of the proposed method using various test examples of heat transfer problems. The obtained results demonstrate that our enriched finite element method preserves the expected efficiency as well as the accuracy. Concluding remarks are summarized in section 5.

## 2 Governing equations for nonlinear transient heat transfer

The transient heat transfer in a composite material in three space dimensions satisfies the nonlinear heat conduction equation

$$\rho(u, t, \mathbf{x})c(u, t, \mathbf{x})\frac{\partial u(t, \mathbf{x})}{\partial t} - \nabla \cdot \left( \kappa(u, t, \mathbf{x})\nabla u(t, \mathbf{x}) \right) = f(u, t, \mathbf{x}), \quad (t, \mathbf{x}) \in (0, \mathcal{T}] \times \Omega, \quad (1)$$

where  $\Omega \subset \mathbb{R}^3$  is the considered computational domain,  $u(t, \mathbf{x})$  is the temperature at point  $\mathbf{x} \in \Omega$  in time  $t \in (0, \mathcal{T}]$ . The function  $f(u, t, \mathbf{x})$  describes the nonlinear reaction term accounting for sources or/and sinks. The material properties  $\kappa, \rho$  and  $c$  are the thermal conductivity, the density and the specific heat, respectively. The boundary and the initial conditions for equation (1) are given as

$$\kappa(u, t, \mathbf{x})\frac{\partial u(t, \mathbf{x})}{\partial \mathbf{n}} + u(t, \mathbf{x}) = g(u, t, \mathbf{x}), \quad (t, \mathbf{x}) \in [0, \mathcal{T}] \times \Gamma, \quad (2)$$

$$u(0, \mathbf{x}) = u_0(\mathbf{x}), \quad \mathbf{x} \in \Omega, \quad (3)$$

with  $\Gamma$  being the domain boundary and  $\mathbf{n}$  the outward unit normal on  $\Gamma$  while  $u_0(\mathbf{x})$  is a prescribed initial temperature and  $g(u, t, \mathbf{x})$  expresses any boundary heat sources or/and sinks. As mentioned earlier, numerical solutions of the nonlinear initial value problem described by (1)-(3) can be computationally demanding especially with the presence of boundary layers and moving fronts, see for example [28].

To solve the problem we use finite elements for the spatial discretization and a semi-implicit scheme for the time integration. Thus, we multiply equation (1) with a test function  $\phi(\mathbf{x})$  before we integrate over the domain  $\Omega$ . After applying the divergence theorem and substituting the boundary conditions we obtain the following weak form

$$\int_{\Omega} \rho c \frac{\partial u}{\partial t} \phi \, d\Omega + \int_{\Omega} \kappa \nabla u \cdot \nabla \phi \, d\Omega = \int_{\Omega} f \phi \, d\Omega + \oint_{\Gamma} (g - u) \phi \, d\Gamma. \quad (4)$$

Next, the domain is discretized into a set of conforming finite elements  $\mathcal{T}_i$ , with  $i = 1, 2, \dots, N_e$  where  $N_e$  is the total number of elements. The computational domain  $\Omega_h \subseteq \Omega$  is the combination of all these elements. The solution  $u(t, \mathbf{x})$  of the weak formulation (4) can then be approximated as

$$u(t, \mathbf{x}) \approx u_h(t, \mathbf{x}) = \sum_{j=1}^{N_d} u_j(t) N_j(\mathbf{x}), \quad (5)$$

with  $N_d$  being the total number of nodes in the computational domain  $\Omega_h$  and  $u_j$  the nodal values of the approximate solution  $u_h(\mathbf{x}_j)$ , while  $\{N_j\}_{j=1}^{N_d}$  are the standard polynomial basis functions.

Next, the time domain is also discretized into uniform timesteps  $[t_n, t_{n+1}]$  of the duration  $\Delta t = t_{n+1} - t_n$  with  $n = 0, 1, \dots, N_t$  and  $N_t = \frac{\mathcal{T}}{\Delta t}$ . We denote a generic function  $w$  with  $w^n$  at the time  $t_n = n\Delta t$ . The integral over the time domain is then performed using a semi-implicit scheme of Gear type also known in the literature by backward differentiation formula (BDF2). Hence, the discrete formulation can be written as

$$\int_{\Omega} \rho^n c^n \frac{3u_h^{n+1} - 4u_h^n + u_h^{n-1}}{2\Delta t} \phi \, d\Omega + \int_{\Omega} \kappa^n \nabla \phi \nabla u_h^{n+1} \, d\Omega + \int_{\Gamma} (u_h^{n+1} - g^{n+1}) \phi \, d\Gamma = \int_{\Omega} f^{n+1} \phi \, d\Omega. \quad (6)$$

Obviously, to advance the solution  $u^{n+1}$  in time, the two solutions  $u^{n-1}$  and  $u^n$  are required. At time  $t = 0$  only one initial condition is provided and to obtain the second condition we use the implicit Euler scheme. If the finite element basis functions *i.e.*  $N_j$  are also used as a test function in (6) then the resulting linear system can be written as

$$\sum_{j=1}^{N_d} \left( \int_{\Omega} \left( \rho^n c^n N_i N_j + 2\Delta t \kappa^n \nabla N_i \cdot \nabla N_j \right) \, d\Omega + \int_{\Gamma} 2\Delta t (N_j - g^{n+1}) N_i \, d\Gamma \right) u_j^{n+1} = \int_{\Omega} \left( 2\Delta t f^{n+1} + \rho^n c^n (4u_h^n - u_h^{n-1}) \right) N_i \, d\Omega, \quad i = 1, 2, \dots, N_d. \quad (7)$$

It should be noted that in the considered semi-implicit scheme, the nonlinear terms at the current time  $t_n$  and therefore only linear systems of algebraic equations are required to update the solution at the next time  $t_{n+1}$ . Thus, the set of equations (7) can be written in a compact form as a linear system of equations

$$\sum_{j=1}^{N_d} a_{i,j} u_j^{n+1} = b_i, \quad i = 1, 2, \dots, N_d, \quad (8)$$

where

$$a_{i,j} = \int_{\Omega} \left( \rho^n c^n N_i N_j + 2\Delta t \kappa^n \nabla N_i \cdot \nabla N_j \right) d\Omega + \int_{\Gamma} 2\Delta t (N_j - g^{n+1}) N_i d\Gamma,$$

$$b_i = \int_{\Omega} \left( 2\Delta t f^{n+1} + \rho^n c^n (4u_h^n - u_h^{n-1}) \right) N_i d\Omega,$$

or simply in matrix form as

$$\mathbf{A} \mathbf{u}^{n+1} = \mathbf{b}, \quad (9)$$

where  $\mathbf{A} = \mathbf{A}(t_{n+1}, \mathbf{u}^n)$  is  $N_d \times N_d$ -valued matrix with entries  $a_{i,j}$ ,  $\mathbf{u}$  and  $\mathbf{b} = \mathbf{b}(t_{n+1}, \mathbf{u}^{n-1}, \mathbf{u}^n)$  are  $N_d$ -valued vectors with entries  $u_i^{n+1}$  and  $b_i$ , respectively. Note that, the linear system must be evaluated and solved at every timestep. Therefore the solution process can be highly demanding computationally if the system involves a large number of equations. Often low-order polynomial basis functions are used for the standard finite element approximations which requires a large number of degrees of freedom. This yields the solution prohibitively expensive in terms of computations. Alternatively we propose using high-order basis functions which can significantly reduce the number of required unknowns, hence, much smaller linear systems to be solved during the time integration procedure.

### 3 Enriched finite element approximations

In the current study, the conventional Lagrangian basis functions are considered for the standard finite element approximation. Both 4-noded tetrahedra and 8-noded hexahedra elements are used. Hence, the polynomial shape function  $N_i(x_j)$  in the expression (5) are linear on each face of a tetrahedra while they are bilinear for each face of a hexahedra element. Notice that the basis functions are characterized by the usual Lagrangian condition of  $N_i(x_j) = \delta_{ij}$  where  $\delta_{ij}$  is the Kronecker delta.

For the partition of unity enrichment [19, 20], the nodal values of the temperature solution  $u_j$  in equation (5) are expanded into a combination of exponential functions as

$$u_j(t) = \sum_{q=1}^Q \varphi_{j,q}(t) \mathcal{G}_q(\mathbf{x}), \quad (10)$$

where

$$\mathcal{G}_q(\mathbf{x}) = \frac{\exp\left(-\left(\frac{\|\mathbf{x} - \mathbf{x}_c\|}{\gamma}\right)^q\right) - \exp\left(-\left(\frac{\beta}{\gamma}\right)^q\right)}{1 - \exp\left(-\left(\frac{\beta}{\gamma}\right)^q\right)}, \quad q = 1, 2, \dots, Q, \quad (11)$$

where  $\beta$  and  $\gamma$  are constants while  $\|\mathbf{x} - \mathbf{x}_c\| = \sqrt{(x - x_c)^2 + (y - y_c)^2 + (z - z_c)^2}$  is the distance between the two points  $\mathbf{x}_c = (x_c, y_c, z_c)^\top$  and  $\mathbf{x} = (x, y, z)^\top$ . The point  $\mathbf{x}_c$  is fixed at the center of the Gaussian function while  $\mathbf{x}$  is a given point in the computational domain. Usually, a set of homogeneous solutions of the considered partial differential equation is chosen for the enrichment [27, 17]. This is often referred to as a set of T-complete functions in the context of Trefftz methods [24]. It is also possible to choose the enrichment functions because they provide improved approximation properties compared to the standard polynomial

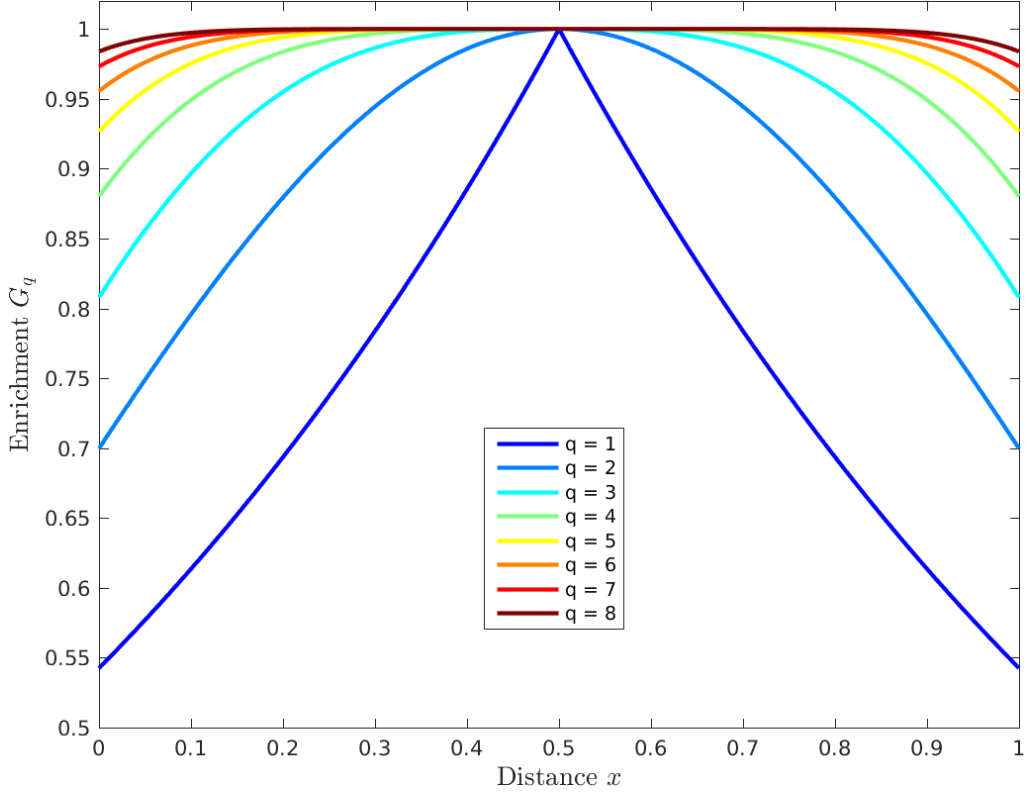


Figure 1: Illustration of the enrichment functions  $\mathcal{G}_q(\mathbf{x})$  defined in (11) for different values of  $q$  plotted for varying  $x$  and keeping  $y = z = 1$  fixed.

basis functions [2]. The enrichment functions (11) are chosen because they represent the temporal variation of the solution at different phases. The partition of unity approximation is then a linear combination of all these functions which at any time instant can be written as

$$u_h(t, \mathbf{x}) = \sum_{j=1}^{N_d} \sum_{q=1}^Q \varphi_{j,q}(t) N_j(\mathbf{x}) \mathcal{G}_q(\mathbf{x}), \quad (12)$$

The unknown  $\varphi_{j,q}$  represents the amplitude of the  $q$ th enrichment function at the  $j$ th node and replaces the unknown nodal value of the temperature  $u_j$  at this node. Increasing the number of enrichment  $Q$  in (12) would add functions with steeper gradients into the approximation. For illustration purposes, we show in Figure 1 the one-dimensional cross-sections at  $y = z = 1$  of the enrichment functions  $\mathcal{G}_q$  for  $q = 1, 2, \dots, 8$  using  $\mathbf{x}_c = (0.5, 0.5, 0.5)^\top$  and the following parameters

$$\beta = \sqrt{\frac{14}{1.195}}, \quad \gamma = \frac{1}{1.195}.$$

As it can be seen in Figure 1 the enrichment functions with low values of  $q$  have sharper gradients than those with high values of  $q$ . Note that similar enrichment functions have been considered in [5] using a-posteriori error estimate for the partition unity finite element method. In addition, the usual stability and conditioning features discussed in [26] are also inherited in this class of enrichment functions.

It should be stressed that the number of degrees of freedom at each mesh node is expanded by the number of enrichment functions  $Q$  in the partition of unity approximation compared to the conventional finite element methods. However, the total number of degrees of freedom and therefore the size of the linear system (9) in the partition of unity method, remains much smaller thanks to the coarse mesh grids used in this case.

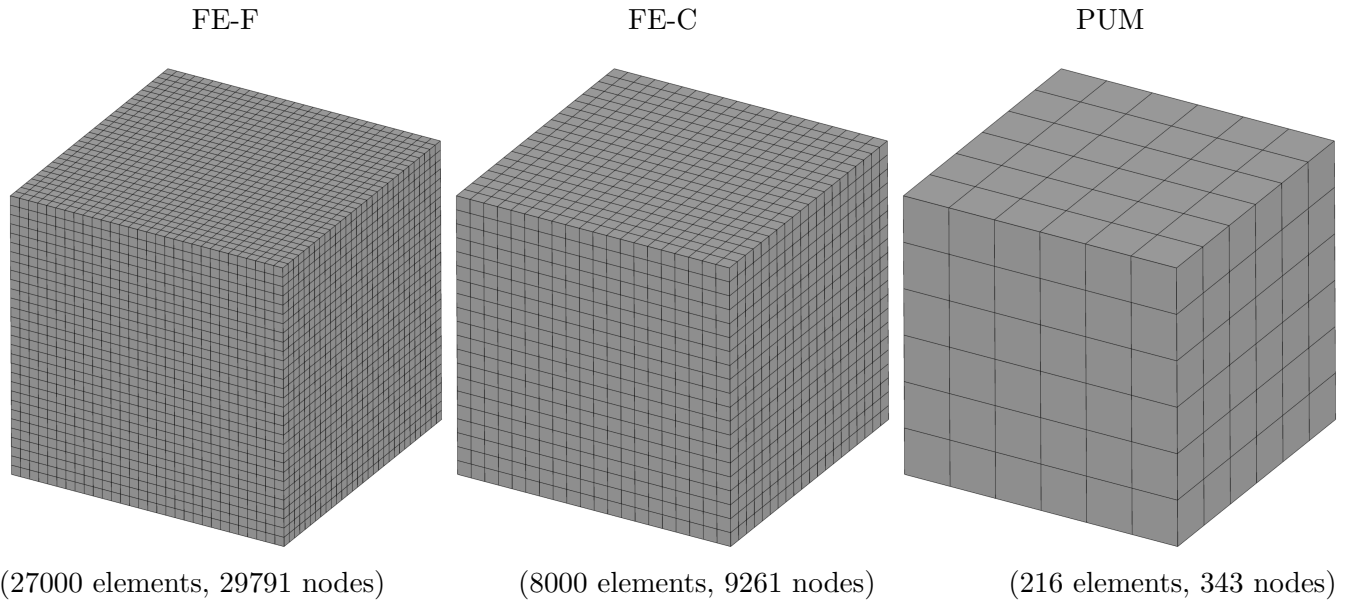


Figure 2: Structured fine mesh used in FEM (left), coarse mesh used in FEM (middle) and coarse mesh used in PUM (right) for the accuracy test.

For the computational results presented in this study, the resulting linear systems are solved using an LU decomposition. It is also worth to mention that a comparison between the structures of matrices associated with linear systems in the FEM and PUM can be found in [18].

## 4 Numerical results

To evaluate the performance of the partition of unity method we consider four different numerical tests. First a manufactured problem with a known exact solution is considered where the heat conductivity is dependent on the temperature. This example is useful for evaluating the performance of the method in terms of errors compared to the standard FEM. In the second example, a problem of heat transfer in ceramic materials is considered where all the material properties such that the thermal conductivity, the density and the specific heat are temperature dependent. In the third problem we consider a functionally graded material composed of a ceramic and a Titanium-Aluminium alloy for which solutions obtained using the PUM on coarse meshes are investigated. In the final example, an industrial application of heat transfer is simulated in a pump part made of a composite materials. Notice that to reduce the computational cost, the timesteps  $\Delta t$  are chosen as large as possible. This makes most explicit time stepping methods noncompetitive, since they are subject to stability restriction conditions. Therefore, the criteria of choosing time steps in our algorithm was mainly based on accuracy considerations. All the computations were performed on an Intel i7-2600 Quad Core at 2.7Ghz and 16GB RAM using Fortran 95 in sequential codes.

### 4.1 Accuracy example with known analytical solution

The PUM is used to solve the nonlinear diffusion problem (1) in the unit cubic domain  $\Omega = [0, 1] \times [0, 1] \times [0, 1]$  with the density and the specific heat coefficients set to unity while the heat conductivity is assumed to nonlinear defined as

$$\kappa(u) = 0.005u^2 + 1.$$

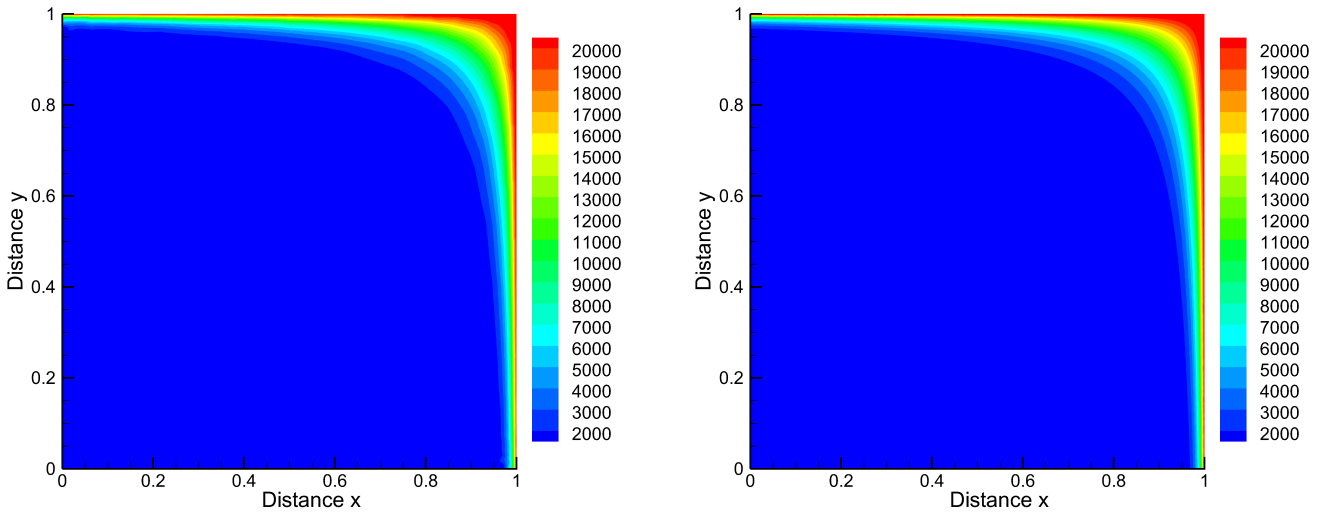


Figure 3: PUM solution on a coarse mesh (left) and exact solution (right) in the  $xy$ -plane at  $z = 0.5$  for the accuracy test example at  $t = 0.1$  using  $\Delta t = 0.05$ .

The following exact solution is imposed on this test problem

$$U(t, x, y, z) = \exp\left(\frac{1}{0.1 + (1-x)(1-y)(1-z)}\right) \left(2 - \exp(-t)\right), \quad (13)$$

and we define the source functions  $g(u, t, \mathbf{x})$  and  $f(u, t, \mathbf{x})$  as well as the initial condition  $u_0(\mathbf{x})$  based on this analytical solution. The problem is also solved with the standard FEM and numerical approximations and both methods are compared using the relative  $L^2$ -error norm defined as

$$\varepsilon_2 = \frac{\|u - U\|_{L^2(\Omega)}}{\|U\|_{L^2(\Omega)}}, \quad (14)$$

where  $\|\cdot\|_{L^2(\Omega)}$  is the  $L^2$ -norm,  $u$  and  $U$  are the computed and the exact solutions, respectively.

In Figure 2 we illustrate the structured meshes used for this test example. Here, a fine mesh (FE-F) composed of 27000 elements and 29791 nodes and a coarse mesh (FE-C) of 8000 elements and 9261 nodes are used for the FEM solution while the coarse mesh with 216 elements and 343 nodes is used for the PUM solution. The aim of this test example is to compare the obtained results using the PUM on a coarse mesh to those obtained using the FEM on a fine mesh. To this end we use the enrichment functions (11) with  $\mathbf{x}_c = (0.5, 0.5, 0.5)^\top$  and

$$\beta = \sqrt{\frac{14}{1.195}}, \quad \gamma = \frac{1}{1.195}.$$

It is evident that this test example exhibits boundary layers at  $x = 1$ ,  $y = 1$  and  $z = 1$ . To illustrate these features, we present in Figure 3 cross-sections in the  $xy$ -plane at  $z = 0.5$  of the exact solution and the PUM solution on a coarse mesh using  $Q = 5$ . As can be seen, the boundary layers are accurately resolved using the PUM on the coarse mesh and no noticeable differences are visible in Figure 3 between the exact solution and the solution obtained using PUM.

Table 1 shows the errors of the solution obtained using the FEM at the two selected instants  $t = 0.05$  and  $0.1$  and using the time step  $\Delta t = 0.001$ . The time step was chosen based on a convergence study where using a smaller time step does not reduce the error for the considered spatial discretization. In this table

Table 1: Relative errors obtained using the PUM and FEM methods on the considered meshes for the accuracy test problem using different numbers of enrichments  $Q$  and  $\Delta t = 0.001$ .

$Q$	$t = 0.05$			$t = 0.1$		
	PUM	FE-C	FE-F	PUM	FE-C	FE-F
3	1.2656E-01	1.8327E-01	1.1426E-02	1.2876E-01	1.9142E-01	1.2131E-02
4	3.3654E-02	1.8327E-01	1.1426E-02	3.3923E-02	1.9142E-01	1.2131E-02
5	7.0536E-03	1.8327E-01	1.1426E-02	7.2638E-03	1.9142E-01	1.2131E-02
6	6.3232E-03	1.8327E-01	1.1426E-02	6.7554E-03	1.9142E-01	1.2131E-02

Table 2: Computational costs in seconds and condition numbers obtained using the PUM and FEM on the considered meshes for the accuracy test problem using different numbers of enrichments  $Q$  and  $\Delta t = 0.001$ .

	CPU time			Condition number
	build/rebuild	solve/resolve	total	
FE-F	32570.51	79.79	39213.11	8.2426
FE-C	9641.20	23.64	11615.84	8.3249
PUM $Q = 3$	236.40	0.068	342.67	2.9258E+05
PUM $Q = 4$	237.66	0.16	373.94	4.0543E+08
PUM $Q = 5$	239.54	0.31	403.76	4.1527E+12
PUM $Q = 6$	241.53	0.54	440.86	2.3675E+13

we also show the relative errors obtained using the PUM for an increased number of enrichment functions. Using the PUM and for the total number of degrees of freedom  $343 \times 5 = 1715$  the error at  $t = 0.05$  is  $\varepsilon_2 = 7.0536 \times 10^{-3}$  compared to  $\varepsilon_2 = 1.1426 \times 10^{-2}$  with the FEM using 29791 degrees of freedom. For a much smaller total number of degrees of freedom, the PUM yields an order of magnitude improvement in the error compared to the FEM. Increasing the number of enrichment functions to  $Q = 6$  it leads to another order of magnitude improvement in the error. In this case, the error is reduced to  $\varepsilon_2 = 6.3232 \times 10^{-3}$  for the total number of degrees of 2058 which is still much smaller than those obtained using the conventional FEM. Similar conclusions can be drawn from the results obtained at later time  $t = 0.1$ .

In Table 2 we summarize the computational costs in terms of CPU times (given in seconds) for the simulations listed in Table 1. Due to the significantly high number of elements, the computational time needed to build the FEM system matrix is two orders of magnitude higher than that for the PUM. The same is also observed for updating the right hand side at later time steps. The resulting linear systems of equations is solved using the LU decomposition. Again because the dimension of system matrix is much smaller when using the PUM, the time needed to perform the decomposition is much shorter than the FEM case. It should be noted that, increasing the number of enrichment functions leads to marginal change in the computational time for building the linear system. It should also be pointed out that Gauss quadratures are used to evaluate the entries of the elementary matrices and in our simulations, the number of integration points used is 20 per direction. This large number of integration points dominates the time needed to evaluate the system matrix. Increasing the number of enrichment functions leads to a clear increase in the time needed to perform building and solving the associated linear systems. This is expected because of the larger linear systems resulting at higher number of enrichment functions. However, for all the considered number of enrichment functions, the computational time remains smaller than the FEM case. Finally, we

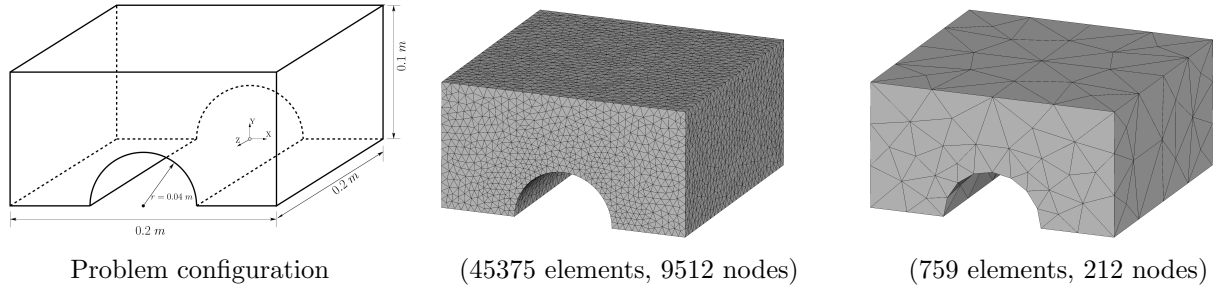


Figure 4: Configuration (left), the considered mesh in the FEM (middle) and for in PUM (right) for the nonlinear transient heat transfer in a homogeneous material.

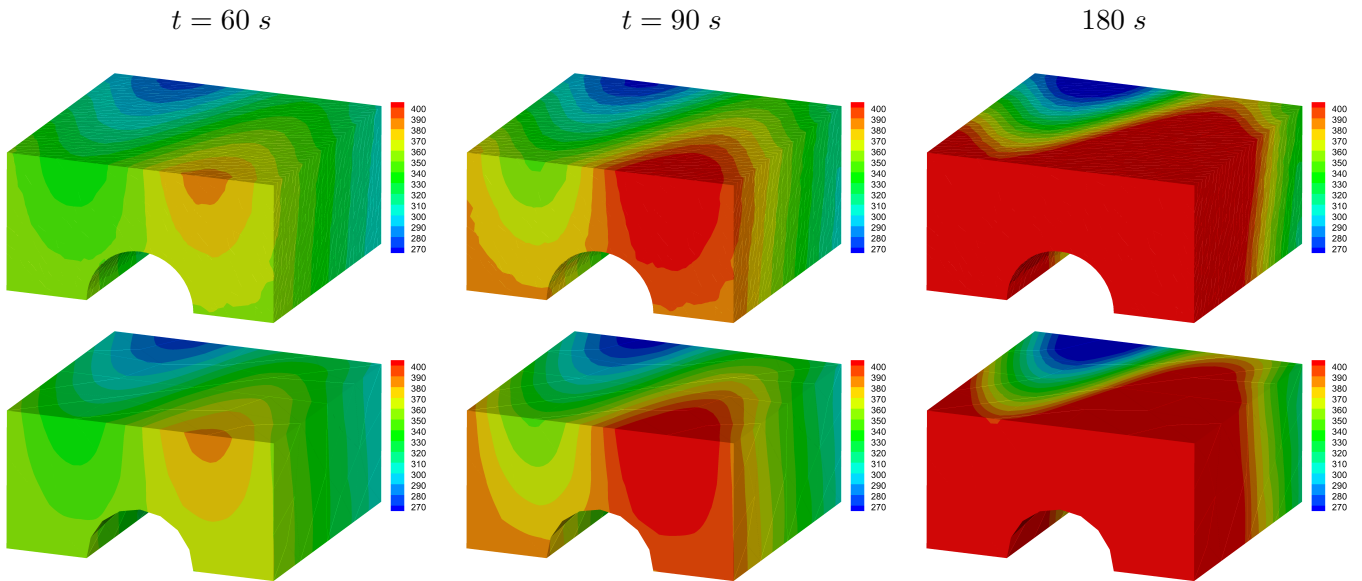


Figure 5: Distributions of the temperature obtained using the FEM on a fine mesh (first row) and the PUM on a coarse mesh (second row) at three different instants for the nonlinear transient heat transfer in a homogeneous material.

also show in Table 2 the total computational time needed to recover the full time span of the problem up to  $t = 0.1$ . It is evident that using the PUM yields a major reduction in the computational time and a significant improvement in the accuracy compared to the standard FEM. The high condition numbers associated with linear system for the PUM in Table 2 should also be noted. The ill-conditioning and the growth of condition numbers in the PUM is well known and have been covered in many studies, see for instance [12, 1]. It should be pointed out that the performance of the proposed PUM is very attractive since the computed solutions remain stable and accurate even when coarse meshes are used without requiring nonlinear solvers or complicated techniques to reconstruct time-dependent enrichment functions.

## 4.2 Nonlinear transient heat transfer in a homogeneous material

In the second example we consider a cube with a cylindrical hole in the center. The cube side length is 20 cm while the cylinder axis is parallel to the  $z$ -axis and has a 4 cm radius. The initial temperature in the domain is  $u_0(\mathbf{x}) = 300$  K. The surrounding ambient temperature is fixed at  $g(u, t, \mathbf{x}) = 300$  K. A heat

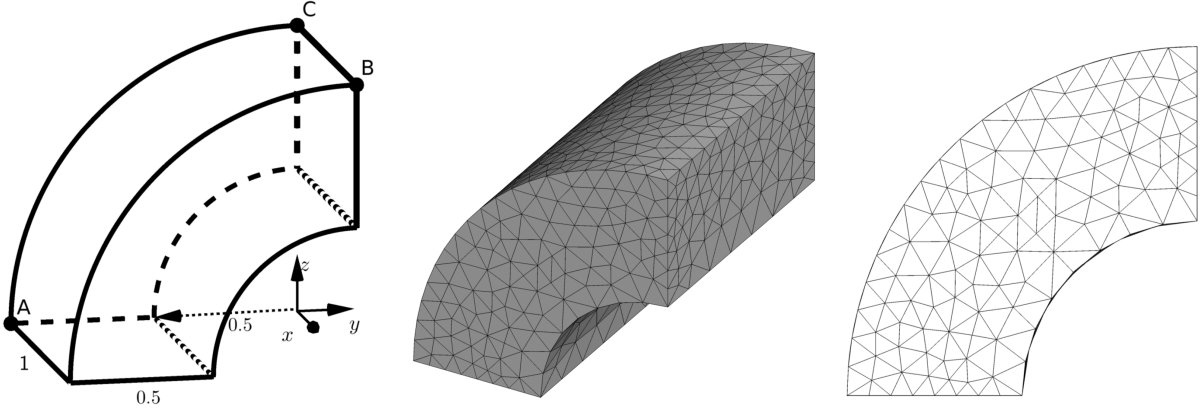


Figure 6: Configuration of the problem (left), the mesh used in the simulations (middle) and side view of the mesh (right) for the nonlinear transient heat transfer in a functionally graded material.

source is introduced into the model defined by  $f(u, t, \mathbf{x})$

$$f(x, y, z) = 5 \times 10^6 \left( z + y \cos(10\pi x) \right) \quad [W/kg]. \quad (15)$$

The cube is made of the Zirconium dioxide ( $ZrO_2$ ) ceramic where the material properties of  $ZrO_2$  are given as

$$\begin{aligned} \kappa(u, t, \mathbf{x}) &= 1.71 + 2.1 \times 10^{-4}u + 1.16 \times 10^{-7}u^2 \quad [W/(mK)], \\ c(u, t, \mathbf{x}) &= 2.74 \times 10^2 + 7.95 \times 10^{-1}u - 6.19 \times 10^{-4}u^2 + 1.71 \times 10^{-7}u^3 \quad [J/(kgK)], \\ \alpha(u, t, \mathbf{x}) &= 1.331 \times 10^{-5} - 1.89 \times 10^{-8}u + 1.27 \times 10^{-11}u^2 \quad [1/K], \\ \rho(u, t, \mathbf{x}) &= \frac{3657}{(1 + \alpha(u - 300))^3} \quad [kg/m^3]. \end{aligned}$$

Note that the problem is symmetric with respect to the  $xz$ -plane. Therefore only half of the domain needs to be considered. Figure 4 illustrates the geometry used in our simulations for this problem. It should be noted that a similar example but in two space dimensions was first introduced in [8]. The problem is solved using the PUM on a coarse mesh grid using the enrichment functions (11) with  $Q = 4$ ,  $\mathbf{x}_c = (0, 0.05, 0.1)^\top$  and

$$\beta = \sqrt{\frac{14}{1.195}}, \quad \gamma = \frac{1}{1.195}.$$

Because no analytical solution is available, the PUM solution is compared to a reference FEM solution evaluated on a fine mesh grid. Figure 4 shows the considered mesh grids and their corresponding number of nodes and elements. The timestep size is fixed at  $\Delta t = 5$  s and simulations are carried out in the time domain  $[0, 180$  s]. The numerical solutions of the PUM as well as the FEM are displayed in Figure 5. The results are displayed at the time instants  $t = 60$  s,  $90$  s and  $180$  s. The heat transfer patterns obtained with the PUM at these time instants are displayed in Figure 5 below those corresponding to FEM. The computed results clearly demonstrate the accuracy of the proposed PUM as the patterns obtained with both PUM and FEM methods are very similar although the PUM uses less than 10 % of the total number of degrees of freedom used in the FEM. Moreover, it can be seen in the figure that the FEM solution displays some spurious oscillations as can be seen for example on the front face of the cube at  $t = 60$  s and  $90$  s while the PUM solutions do not show such oscillations.

### 4.3 Nonlinear transient heat transfer in a functionally graded material

In the third example we study the heat transfer in a functionally graded material composed of the Zirconium dioxide ceramic and a Titanium alloy (Ti 6Al-4V). The material properties considered for  $ZrO_2$  are similar

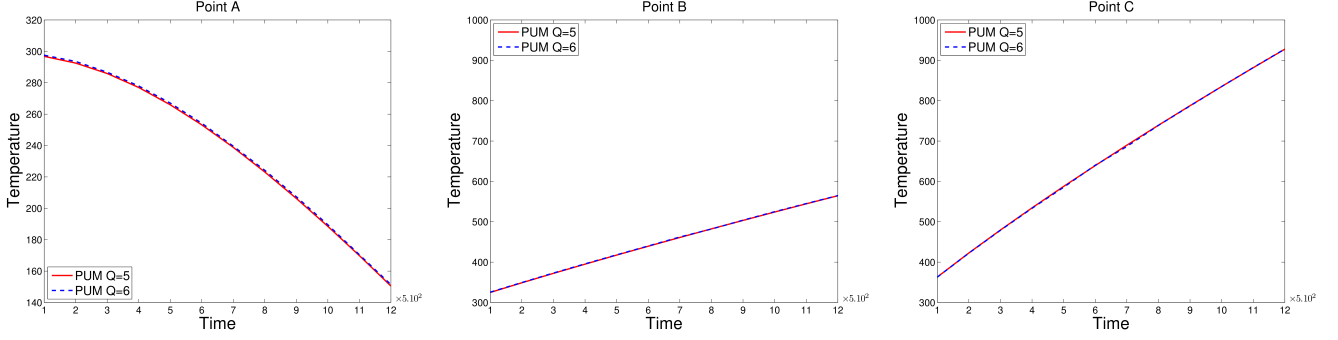


Figure 7: Time evolution of the temperature at points A, B and C for the nonlinear transient heat transfer in a functionally graded material.

to the previous example while for Ti 6Al-4V they are given by

$$\begin{aligned}
 \kappa(u, t, \mathbf{x}) &= 1.1 + 1.7 \times 10^{-2}u \quad [W/(mK)], \\
 c(u, t, \mathbf{x}) &= 3.5 \times 10^2 + 8.78 \times 10^{-1}u - 9.74 \times 10^{-4}u^2 + 4.43 \times 10^{-7}u^3 \quad [J/(kgK)], \\
 \alpha(u, t, \mathbf{x}) &= 7.43 \times 10^{-6} + 5.56 \times 10^{-9}u - 2.69 \times 10^{-12}u^2 \quad [1/K], \\
 \rho(u, t, \mathbf{x}) &= \frac{4420}{(1 + \alpha(u - 300))^3} \quad [kg/m^3].
 \end{aligned}$$

The heat source is defined as

$$f(x, y, z) = 1.5 \times 10^5 \left( y + (x^2 + y^2 + z^2) \exp\left(-x \frac{\pi}{2}\right) \right) \quad [W/kg]. \quad (16)$$

The considered computational domain is a quarter of a cylinder with an axial hole. Figure 6 shows the geometrical configuration of the domain. The material properties of the composite are evaluated at each point using the mixture rule

$$p = p_1 \xi_1 + p_2 \xi_2, \quad (17)$$

where the volume fractions of the ceramic and the alloy are respectively  $\xi_1$  and  $\xi_2$ , whereas  $p_1$  and  $p_2$  are the corresponding material properties. The percentage of the alloy volume fraction starts at a 100% on the inner surface of the cylinder and decreases to 0 on the outer surface while the ceramic volume fraction increases at the same rate so that

$$\xi_1 = 2r - 1, \quad \xi_2 = 1 - \xi_1,$$

with  $r$  being the radial coordinate where the origin is located on the cylinder axis at the top face and is depicted in Figure 6. It should be noted that a similar problem was also studied in [8, 13].

It is worth to mention that the aim in this example is to evaluate the convergence of the PUM solution using a fixed mesh and an increased number of enrichment functions. For this test problem the time step is  $\Delta t = 5$  s and the considered computational mesh is shown in Figure 6. For better insight, views of both side and elevation are displayed in this figure next to the configuration. The mesh is composed of 3123 tetrahedral elements and 809 nodes and the enrichment functions (11) are used with  $\mathbf{x}_c = (0.5, 0.1, 0)^\top$  and

$$\beta = \sqrt{\frac{0.525}{0.111}}, \quad \gamma = \frac{1}{0.111}.$$

The problem is solved first using  $Q = 3$  enrichment functions and subsequently this number is increased to 4, 5 and finally 6. The results of each increment is then compared to the previous one. Using five or six enrichment functions lead to very similar results. Hence, we can conclude that the solution has converged

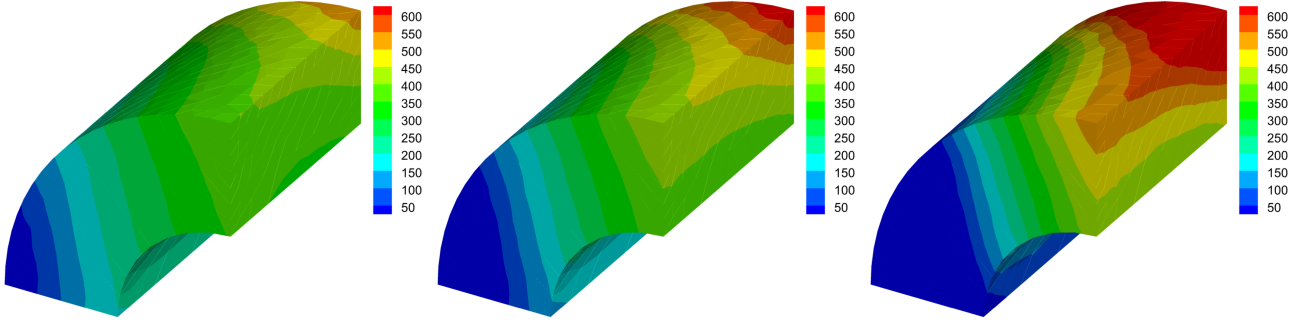


Figure 8: Distributions of the temperature obtained using the PUM at  $t = 2000$  s (left),  $3000$  s (middle) and  $5000$  s (right) for the nonlinear transient heat transfer in a functionally graded material.

Table 3: Comparison of number of DoFs, condition numbers and the maximum temperature (Max) obtained using the PUM at  $t = 2000$  s for the nonlinear transient heat transfer in a functionally graded material.

	DoFs	Condition number	Max
PUM $Q = 4$	3236	2.1093E+14	533.62
PUM $Q = 5$	4045	8.8437E+16	533.40
PUM $Q = 6$	4854	1.0709E+18	533.46

at five enrichment functions. Figure 7 shows the time evolution in the temperature at the points A, B and C located at  $(0, -1, 0)$ ,  $(1, 0, 1)$  and  $(0, 0, 1)$ , respectively. These points are also highlighted on the domain configuration in Figure 6. The time evolution shows that the temperature obtained using  $Q = 5$  or  $Q = 6$  are similar for the full time domain and at all the considered points. Figure 8 shows the converged solution with five enrichment functions at the instants  $t = 2000$  s,  $3000$  s, and  $5000$  s. Again the PUM performs very well for this test example of nonlinear transient heat transfer in a functionally graded material. Needless to say that for this heat transfer situation, the PUM does not introduce excessive numerical dissipation or exhibits spurious oscillations near the steep thermal gradients. In table 3 we summarize the number of DoFs, condition numbers and the maximum temperature (Max) obtained using the PUM with  $Q = 4, 5$  and  $6$  at  $t = 2000$  s. It is evident that, increasing the number of enrichments in the PUM yields an increase in the number of DoFs along with a substantial increase in the condition numbers of the matrix associated with linear systems to be solved in the PUM. In terms of values of the maximum temperature, there is little differences between the results obtained using  $Q = 4, 5$  and  $6$ .

#### 4.4 Nonlinear transient heat transfer in a pump part

Our last test example consists of a problem of transient heat transfer in an industrial geometry. We consider a pump part that is formed using a composite of Zirconium dioxide ceramic ( $ZrO_2$ ) and a Titanium alloy (Ti 6Al-4V). The geometry of the part is displayed in Figure 9 and is based on the file `pump_carter_sup.stp` kindly provided by INRIA and available on the shape repository AIM@SHAPE<sup>1</sup>. The thermal properties considered for ( $ZrO_2$ ) and (Ti 6Al-4V) are similar to the previous example. The same mixture rules from the previous example are also considered here. An internal heat source is imposed on the entire computational domain at the rate  $f = 135$  W/kg. Initially, the domain is set at initial temperature of  $u_0 = 200$  K. Heat

<sup>1</sup><http://visionair.ge.imati.cnr.it/ontologies/shapes/>

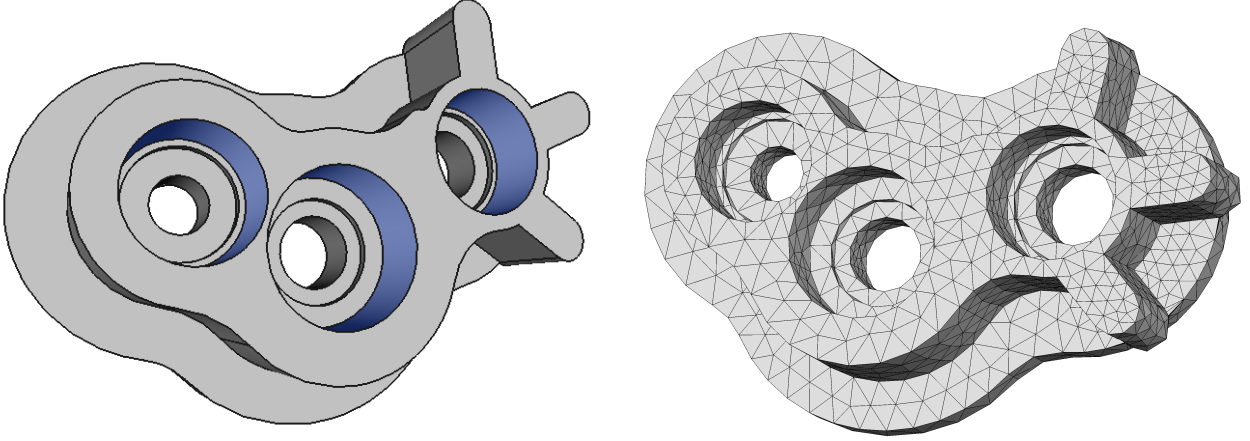


Figure 9: Domain configuration (left) and the mesh (right) used in the PUM for the nonlinear transient heat transfer in a pump part.

isolation is assumed on all surfaces of the pump part except for the inner upper section of the cylindrical surfaces which are highlighted with blue in Figure 9. On these surfaces high heat gradient is imposed so that the heat energy is released at a significant rate on these surfaces. On the rest of boundaries the heat is isolated, hence, no heat transfer is permitted. The corresponding boundary conditions are  $\kappa \frac{\partial u}{\partial \mathbf{n}} = 0$  and  $\kappa \frac{\partial u}{\partial \mathbf{n}} = 293 \text{ K/m}$  on the isolated and non-isolated boundary surfaces, respectively.

The aim now is to test the PUM on a complex geometry that is relevant to an industrial application. To this end the domain is discretized into 4-noded tetrahedral elements composed of 6602 elements and 1882 nodes. The mesh is displayed in Figure 9 along side the geometry. We present numerical results at three different instants using the time step  $\Delta t = 0.1 \text{ s}$ . Here, the enrichment functions (11) are considered with  $c = 1, 2$  and  $3$  for each  $q$  such that the control points  $\mathbf{x}_c$  coincide with the center of each hole in the pump part *i.e.*  $\mathbf{x}_1 = (-118.16, 0, 18)^\top$ ,  $\mathbf{x}_2 = (0, 0, 18)^\top$  and  $\mathbf{x}_3 = (55.44, 63.11, 18)^\top$  and

$$\beta = \sqrt{\frac{14}{1.195}}, \quad \gamma = \frac{1}{1.195}.$$

To test the convergence of the PUM the number of enrichment functions is increased in steps of one from  $Q = 2$  to  $Q = 5$ . For each value of  $Q$ , three center points  $\mathbf{x}_c$  are used so that one point is located at the center of each cylindrical hole. This choice is made as the heat exchange is expected to be high on the inner surfaces of these holes due to the imposed high heat gradients. The obtained results show that the method converges for  $Q = 3$  and adding more enrichment functions would not lead to further changes in the resolution of the computed solutions. Figure 10 shows the converged solution at the instants  $t = 2.5 \text{ s}$ ,  $5 \text{ s}$ ,  $7.5 \text{ s}$  and  $10 \text{ s}$ . As expected the temperature builds up at the domain parts further away from the holes and drops rapidly in the area near the holes. Steep gradients forms in the domain due to the difference between the heat isolation boundary conditions and the high heat release rates near the cylindrical holes. These steep gradients and their change in time are efficiently captured using the enrichment functions despite using a coarse mesh grid. From the computed results we can observe that the complicated heat structures in the pump part captured by the enriched finite element method. It is worth remarking that all these features have been achieved using tetrahedral meshes coarser than those required for conventional finite element methods.

## 5 Conclusions

This paper investigates the nonlinear transient heat transfer in functionally graded materials where particular attention is paid to steep heat gradients. The considered nonlinearity is caused by the material

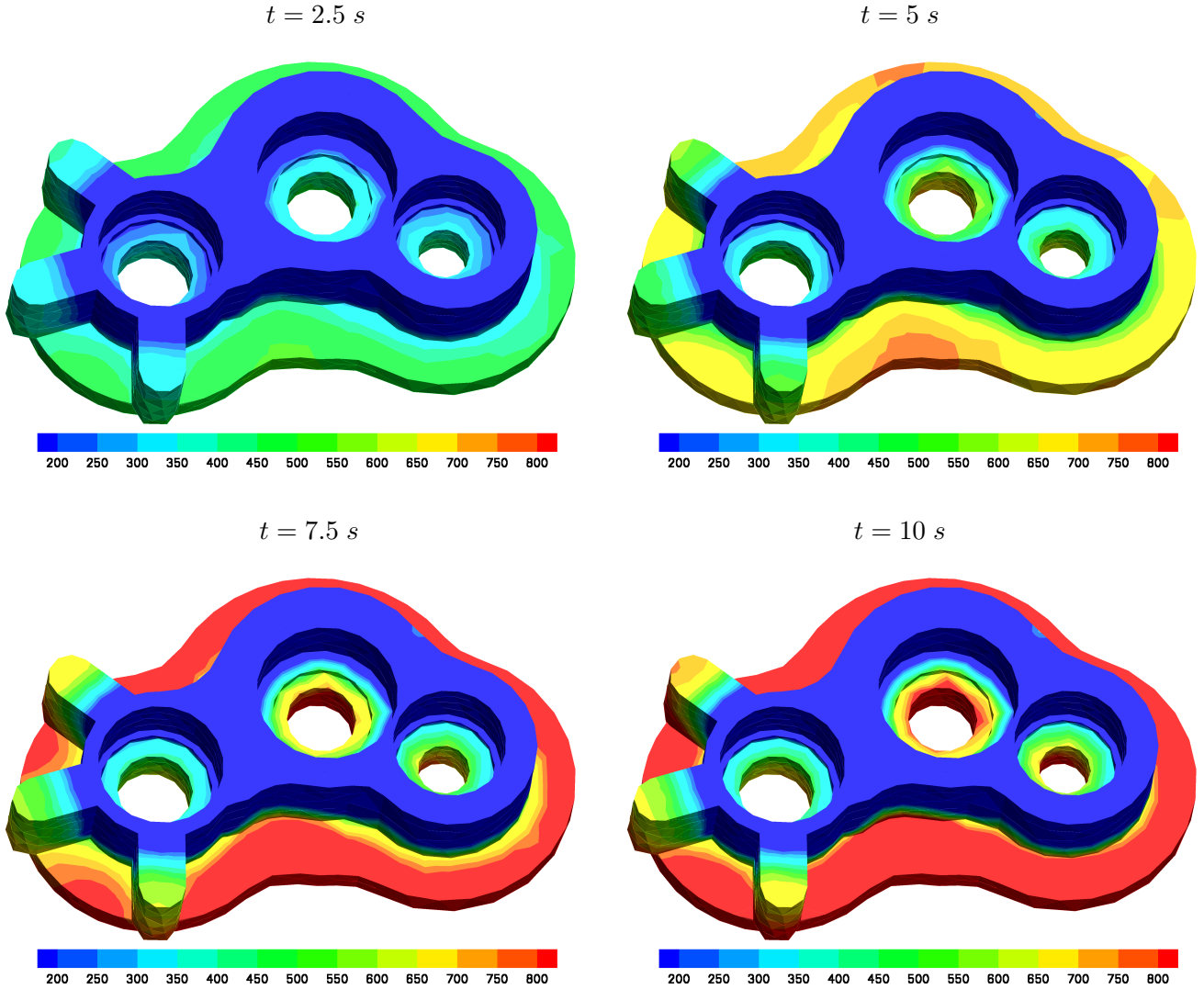


Figure 10: Distributions of the temperature obtained using the PUM for the nonlinear transient heat transfer in a pump part at four different times  $t = 2.5\text{ s}$ ,  $5\text{ s}$ ,  $7.5\text{ s}$  and  $10\text{ s}$ .

properties and/or the behavior of the source/sink terms inside the computational domain. When solving such problems and in order to achieve high engineering accuracy with standard numerical methods it is important to use heavily refined meshes. The resulting high number of degrees of freedom can be computationally demanding especially in time-dependent applications. To deal with this difficulty we propose incorporating time-independent exponential enrichment functions to the finite element approximation using the partition of unity method. Furthermore, to avoid solving a nonlinear system of equations a semi-implicit time integration scheme is used. The proposed approach exploits the advantage of adapting the enrichment locally to capture various features of the solution on a coarse mesh instead of using highly refined meshes. Other enrichment functions accounting for properties of the functionally graded material under study can also be implemented in the proposed formulation without major conceptual modifications. Several numerical experiments are carried out to validate the presented approach. The results show an order of magnitude improvement in the accuracy compared to the standard finite element method. This significant reduction in the error is achieved using an order of magnitude less degrees of freedom. The presented comparisons also show a corresponding reduction in the computational time compared to the standard finite element method. Moreover, we present an enrichment refinement approach to test the convergence of the method where the

number of enrichment functions is increased on a fixed mesh. We show that this approach is more efficient than the standard approach of refining the mesh. The partition of unity method is implemented to recover the heat transfer in a functionally graded material composed of a ceramic and a Titanium alloy in simple and complex geometries for industrial applications. The results confirm the suitability of the proposed method for this type of geometries. Thus, the method can be an attractive approach to replace standard numerical methods such as the finite element method for nonlinear transient heat transfer in functionally graded materials. It should also be stressed that the performance of the partition of unity method is limited with the choice of enrichment functions which depend on the problem under study. Developing a unified strategy to build optimal enrichment functions is still an open question in many applications in science and engineering.

Finally, although the method enables approximating complicated local features of the solution using coarse meshes but in order to have an accurate description of the geometry it may become necessary to use refined meshes. Such an accurate description of the geometry may become a major burden in nonlinear applications. Therefore, in order to have an accurate description of the geometry on coarse meshes it may become necessary in the future to use non-uniform rational B-splines to mesh the domain instead of the Lagrangian polynomials commonly used in the standard finite element methods.

**Acknowledgment.** The authors would like to thank anonymous referees for giving very helpful comments and suggestions that have greatly improved this paper.

## References

- [1] Ivo Babuška and Uday Banerjee. Stable generalized finite element method (sgfem). *Computer methods in applied mechanics and engineering*, 201:91–111, 2012.
- [2] G.C. Diwan, M.S. Mohamed, M. Seaid, J. Trevelyan, and O. Laghrouche. Mixed enrichment for the finite element method in heterogeneous media. *Int. J. Numer. Meth. Engng.*, 101:54–78, 2015.
- [3] C.A. Duarte and D.J. Kim. Analysis and applications of a generalized finite element method with global-local enrichment functions. *Comput. Methods Appl. Mech. Engrg.*, 197:487–504, 2008.
- [4] Z.J. Fu, Q.H. Qin, and W. Chen. Hybrid-Trefftz finite element method for heat conduction in nonlinear functionally graded materials. *Eng. Comp.*, 28:578–599, 2011.
- [5] M. Iqbal, H. Gimperlein, O. Laghrouche, K. Alam, S.M. Mohamed, and M. Abid M. A residual a-posteriori error estimate for PUFEM solutions of 3D transient heat diffusion problems using multiple global enrichment functions. *Int J Numer Methods Eng.*, 2020.
- [6] M. Iqbal, K. Masood, A. Aljuhni, and A. Ahmad. Generalized finite element method with time-independent enrichment functions for 3D transient heat diffusion problems. *Int. J. Hat Mass Transf.*, 149:118969, 2020.
- [7] M. Karkon. Hybrid-Trefftz formulation for analysis of anisotropic and symmetric laminated plates. *Compos. Struct.*, 134:460–474, 2015.
- [8] A. Khosravifard, M.R. Hematiyan, and L. Marin. Nonlinear transient heat conduction analysis of functionally graded materials in the presence of heat sources using an improved meshless radial point interpolation method. *Appl. Math. Model.*, 35:4157–4174, 2011.
- [9] D.J. Kim, S.G. Hong, and C.A. Duarte. Generalized finite element analysis using the preconditioned conjugate gradient method. *Appl. Math. Model.*, 39:5837–5848, 2015.

- [10] H. Li and C.A. Duarte. A two-scale generalized finite element method for parallel simulations of spot welds in large structures. *Comput. Methods Appl. Mech. Engrg.*, 337:28–65, 2018.
- [11] H. Li, P. O’Hara, and C.A. Duarte. A two-scale generalized fem for the evaluation of stress intensity factors at spot welds subjected to thermomechanical loads. *Eng. Fract. Mech.*, 213:21–52, 2019.
- [12] R.M. Lins, M.D.C. Ferreira, S.P.B. Proena, and C.A. Duarte. An a-posteriori error estimator for linear elastic fracture mechanics using the stable generalized/extended finite element method. *Comput. Mech.*, 56(6):947–965, 2015.
- [13] G.R. Liu and X. Han. Computational inverse techniques in nondestructive evaluation. *CRC*, pp:269–271, 2003.
- [14] M. Malek, N. Izem, M.S. Mohamed, M. Seaid, and O. Laghrouche. A partition of unity finite element method for three-dimensional transient diffusion problems with sharp gradients. *J. Comp. Phys.*, 396:702–717, 2019.
- [15] M. Malek, N. Izem, M. Seaid, M.S. Mohamed, and M. Wakrim. A partition of unity finite element method for nonlinear transient diffusion problems in heterogeneous materials. *Comp. Appl. Math.*, 38:31, 2019.
- [16] J.M. Melenk and I. Babuška. The partition of unity finite element method: Basic theory and applications. *Comput. Methods Appl. Mech. Engrg.*, 139:289–314, 1996.
- [17] M.S. Mohamed, A. El-Kacimi, and O. Laghrouche. Some numerical aspects of the PUFEM for efficient solution of 2D Helmholtz problems. *Comput. Struct.*, 88:1484–1491, 2010.
- [18] M.S. Mohamed, M. Seaid, and A. Bouhamidi. Iterative solvers for generalized finite element solution of boundary-value problems. *Numer. Linear. Algebr. with Applications*, 25:e2205, 2018.
- [19] M.S. Mohamed, M. Seaid, J. Trevelyan, and O. Laghrouche. A partition of unity fem for time-dependent diffusion problems using multiple enrichment functions. *Int. J. Numer. Meth. Engrg.*, 93:245–265, 2013.
- [20] M.S. Mohamed, M. Seaid, J. Trevelyan, and O. Laghrouche. Time-independent hybrid enrichment for finite element solution of transient conduction-radiation in diffusive grey media. *J. Comp. Phys.*, 251:81–101, 2013.
- [21] M.S. Mohamed, M. Seaid, J. Trevelyan, and O. Laghrouche. An enriched finite element model with q-refinement for radiative boundary layers in glass cooling. *J. Comp. Phys.*, 258:718–737, 2014.
- [22] P. O’Hara, C.A. Duarte, and T. Eason. Generalized finite element analysis of three-dimensional heat transfer problems exhibiting sharp thermal gradients. *Comput. Methods Appl. Mech. Engrg.*, 198:1857–1871, 2009.
- [23] P. O’Hara, C.A. Duarte, and T. Eason. Transient analysis of sharp thermal gradients using coarse finite element meshes. *Comput. Methods Appl. Mech. Engrg.*, 200:812–829, 2011.
- [24] Q.H. Qin. Hybrid-Trefftz finite element method for reissner plates on an elastic foundation. *Comput. Methods Appl. Mech. Engrg.*, 122:379–392, 1995.
- [25] Q.H. Qin. *The Trefftz finite and boundary element method*. Wit Pr/Comput. Mech., 2000.
- [26] M.A. Schweitzer. Stable enrichment and local preconditioning in the particle-partition of unity method. *Numer. Math.*, 118:137–170, 2011.
- [27] Z. She, K. Wang, and P. Li. Thermal analysis of multilayer coated fiber-reinforced composites by the hybrid Trefftz finite element method. *Compos. Struct.*, 224:110992, 2019.

- [28] J.A. Smoller. *Shock Waves and Reaction-Diffusion Equations*. Springer-Verlag, New York, 1982.
- [29] F.P. van der Meer, R. Al-Khoury, and L.J. Sluys. Time-dependent shape functions for modeling highly transient geothermal systems. *Int. J. Numer. Meth. Engng.*, 77:240–260, 2009.
- [30] J. Xiao, Y. Xu, and F. Zhang. An analytical method for predicting the effective transverse thermal conductivity of nano coated fiber composites. *Compos. Struct.*, 189:553–559, 2018.



**Citation on deposit:** Malek, M., Izem, N., Mohamed M, S., & Seaid, M. (2020). A three-dimensional enriched finite element method for nonlinear transient heat transfer in functionally graded materials. *International Journal of Heat and Mass Transfer*, 155, Article 119804. <https://doi.org/10.1016...asstransfer.2020.119804>

**For final citation and metadata, visit Durham**

**Research Online URL:** <https://durham-repository.worktribe.com/output/1225166>

**Copyright statement:** © 2022. This manuscript version is made available under the CC-BY-NC-ND 4.0 license <https://creativecommons.org/licenses/by-nc-nd/4.0/>